Journal of Nuclear Materials 527 (2019) 151818

Contents lists available at ScienceDirect

Journal of Nuclear Materials

journal homepage: www.elsevier.com/locate/jnucmat

Swelling resistance of advanced austenitic alloy A709 and its comparison with 316 stainless steel at high damage levels

Hyosim Kim [a, b], Jonathan G. Gigax [b], Jiangyuan Fan [a], Frank A. Garner [a], T.-L. Sham [c], Lin Shao [a, *]

[a] Department of Nuclear Engineering, Texas A&M University, TX, 77843, United States
[b] Los Alamos National Laboratory, Los Alamos, NM, 87544, United States
[c] Argonne National Laboratory, Lemont, IL, 60439, United States

ARTICLE INFO

Article history:
Received 12 April 2019
Received in revised form
27 September 2019
Accepted 27 September 2019
Available online 27 September 2019

ABSTRACT

Alloy A709 is an austenitic alloy developed for power boiler applications in thermal power plants and is being considered as a candidate structural material for Generation IV reactors and fusion reactors, based especially on its increased creep strength over Type 316 stainless steel. However, improved thermal creep properties would not necessarily imply improved radiation resistance, especially with respect to void swelling. Since there are currently no neutron irradiation data on A709 to high fluences, A709 and cold-worked 316 were irradiated in the present study under identical conditions to doses between 100 and 400 peak dpa using irradiation by 3.5 MeV Fe^{+2} ions. The swelling behavior of 316 is well-known for both neutron and ion irradiation, thus the relative swelling behavior of A709 and 316 under ion irradiation might provide an indication of the swelling behavior of A709 in a neutron irradiation environment. Swelling of A709 under ion irradiation was observed over the range of 500–600 °C, peaking at 575 °C. Both A709 and 316 eventually swelled at a rate of ~1%/dpa under ion irradiation at 575 °C, consistent with the swelling of 316 observed during neutron irradiation. But A709 had a significantly longer transient regime than 316 at any given dpa rate, demonstrating enhanced swelling resistance of A709 over 316 under self-ion irradiation. The swelling levels reached at 400 peak dpa were 55% and 90% for A709 and 316, respectively. The assigned local dpa levels were adjusted both temporally and spatially at each dose for swelling-induced increases in the ion range and concomitant decreases in density. The duration of the transient regime in each alloy was also observed to increase as the local dpa rate increased, but with a different flux sensitivity that is speculated to arise from the very different composition of the two alloys.

1. Introduction

There have been numerous efforts over the last four decades to develop advanced structural alloys for both light water power reactors and higher-flux fast reactors that can maintain good mechanical properties and dimensional stability under conditions of high temperature, applied stress, flowing corrosive coolant, high radiation damage rates and very high displacement levels. Additionally, radiation-resistant structural materials are required for use in various future fusion power devices. The majority of the developmental and testing efforts for these various reactor concepts have focused primarily on austenitic stainless steels that have previously been used as reactor structural components due especially to their high temperature stability and corrosion resistance in both water and sodium. Unfortunately, the austenitic class of steels have been found to be susceptible to double-digit levels of neutron-induced void swelling at high displacement doses and high temperatures, a phenomenon that is a life-limiting process for reactor components, especially for high-flux fast reactors at high damage levels and high operation temperatures [1–3].

Swelling has also been observed in austenitic steels in pressurized light water reactors where components can receive as much as 70–100 dpa over a 40-year operating time period. Due to the lower operating temperatures (280–380 °C) in these reactors, the observed swelling levels are much lower than those of fast reactors

* Corresponding author.
E-mail address: lshao@tamu.edu (L. Shao).

https://doi.org/10.1016/j.jnucmat.2019.151818
0022-3115/

[1,4,5]. For Generation IV reactors and fusion reactors, however, it is desired that the in-core structural materials (including both metal and ceramic materials) will survive damage levels approaching or exceeding 200 dpa at temperatures that might approach as high as 1000 °C [4,6]. Currently, there are two major approaches being pursued in the development of improved alloys for radiation service under such extreme temperature and dose conditions. The first approach involves the optimization of alloys in the austenitic class and the second involves the use of ferritic/martensitic alloys that are known to swell at much lower rates [3]. This report focuses on the first approach involving an austenitic alloy designed to have improved performance in high temperature non-radiation environments.

It is important to note, however, that demonstrated superior thermal performance of an alloy does not necessarily guarantee superior radiation performance, especially concerning the propensity for void swelling. Therefore, radiation testing in the target neutron environment is necessary to assess whether superior thermal and radiation performance are both attained and most importantly, are both maintained to high dose. Due to the unavailability of high-flux irradiation facilities in the US, only relatively low neutron-induced doses can be explored and most studies to higher damage doses must be conducted using energetic charged particles as surrogates for neutrons. To assess the radiation performance of a previously neutron-untested candidate alloy in the absence of high-flux neutron facilities, we have chosen to use self-ion irradiation, comparing the performance of the new neutron-untested alloy with that of 316 stainless steel under identical irradiation conditions. The latter steel has been used in many previous neutron irradiation experiments and its behavior is well known. Observed differences in ion-induced behavior of the two alloys can then hopefully be extrapolated to anticipate similar differences in neutron-induced behavior, using the 316 results as a reference point.

The Fe−20Cr−25Ni austenitic alloy, A709, which has the same chemical compositions as NF709, is a candidate alloy for service in next-generation sodium-cooled fast reactors (SFRs) due to its high temperature strength, sodium compatibility, oxidation resistance, and weldability [6−14]. NF709 was originally developed in the 1980s as seamless tubing for applications in ultra-supercritical thermal power plants by Nippon Steel Corporation in Japan [15]. It has significantly higher creep strength, close to two times at 700 °C, as compared with the more commonly used Type 316 stainless steel [11−14]. Different processing and heat treatment conditions that balance the creep and creep-fatigue properties of A709 have been developed by the US Advanced Reactor Technologies Program for other product forms, e.g., plates [16−18].

Previous investigations of the radiation response of A709 focused on its mechanical properties [7,9], thermophysical properties [8], and microstructural evolution [9,10,13]. Kim et al. observed no voids in A709 after neutron irradiation to 3 dpa at 500 °C, and reported radiation hardening of 76% resulting from formation of Frank loops and radiation-induced precipitates [9]. Xu and coworkers conducted a study on dislocation loop and precipitate evolution using 1 MeV Kr ions to 3 dpa at various temperatures, and also reported on the absence of voids [13]. Recently, in a companion A709 study conducted for another group on our accelerator, voids were not observed at 10 dpa but were observed at doses of 50 and 150 dpa using 3.5 MeV Fe ions [14,16,19,20].

In the current study, we chose to use Fe^{+2} self-ions as a surrogate instead of protons or heavy ions (Au, Xe, etc.) to better approximate cascade defect distributions produced by neutrons. Additionally, self-ions produce much less heat deposition per dpa than protons, allowing attainment of the higher dpa rates ($>1 \times 10^{-3}$ dpa/s) needed to reach the very high dpa levels required in this study to fully examine the relative swelling behavior of the two alloys [21,22].

The use of self-ions as a surrogate for neutron irradiation is known to require consideration of various neutron-atypical aspects of ions involving sputtering, mass-injection, surface sink effects, defect imbalance distributions, injected interstitial effects, beam-rastering, internal stresses, swelling-induced range extension, beam-induced contamination, and dose rate effects, with the latter consideration addressing dose rate effects both along the ion penetration range and between the neutron and ion irradiation environments [22−31]. The relevant neutron-atypical aspects and their impact on the A709-316 comparison will be addressed as they arise in the Experimental procedure and Discussion sections.

1.1. Experimental procedure

The composition of A709 and 316 is given in Table 1. The as-received A709 (Carpenter Technology Heat #011502, Lot #H4) was forged and hot-rolled, followed by annealing at 1100 °C and water quenching. The 316 stainless steel was derived from an archive reflector block with hexagonal cross-section (52 mm face-to-face, 245 mm length). These blocks were used as fillers in reflector assemblies of the EBR-II fast reactor in Idaho Falls, ID, USA. The thermo-mechanical starting condition of these 316 blocks was not specified in the production order but is thought to be lightly cold-worked, perhaps on the order of ~5% cold-worked, since comparable 304 blocks produced by the same vendor were found to have ~5% cold-work inside the block and ~10% surface working [32,33]. Microscopy shown in Fig. 1 of the as-received 316 used in this study indeed showed that the internal microstructure was representative of light cold-working, although the exact level cannot be specified.

The A709 and 316 specimens were sectioned into 5 mm × 5 mm × 0.75 mm pieces and then mechanically polished using SiC paper to a grit of 1200 (P-4000). The samples were subsequently polished using a 0.25 μm diamond solution with a final polishing step using 0.04 μm silica. The surfaces of the polished specimens were imaged using a TESCAN Lyra scanning electron microscope (SEM) prior to irradiation to ensure that a clean flat surface was produced.

Heavy ion irradiations using 3.5 MeV Fe^{2+} ions were performed with a 1.7 MV Ionex Tandem Accelerator at the Texas A&M Ion Beam Lab. A static, defocused beam was utilized to avoid the effects of strong void suppression arising from beam rastering [34,35]. The temperature of the specimens was monitored using calibration and measurement techniques described in a previous paper [34], and it was found to be stable at ±3 °C throughout the irradiation.

The dpa profiles and implanted ion profiles were calculated using the Kinchin-Pease option of the SRIM-2013 code with a displacement energy of 40 eV for all major compositional elements [36,37]. A recently-developed ion beam filtering system using a series of deflecting magnets and a liquid nitrogen cold trap on the beam line was used to avoid beam-induced contamination (C-, N-, O-rich molecules) of the specimens during irradiation [23,38−40]. Beam-induced carbon contamination especially, and its consequences on swelling and phase stability, has also received increased attention from other researchers [41−45]. The target chamber pressure was maintained at 6×10^{-8} torr or better during irradiation with assistance of a liquid nitrogen cold trap located at the chamber.

Gas implantation (He, H, etc.) was not employed in this irradiation series. Specimens of A709 were first irradiated to 200 peak dpa at temperatures of 500, 525, 550, 575, and 600 °C to determine the peak swelling temperature. This temperature was found to be 575 °C. Thereafter A709 was irradiated to 100, 200, 250, 300, 350,

Table 1
Chemical compositions of A709 and 316 (wt %).

	Fe	Ni	Cr	Mo	Mn	Si	Nb	N	C	Ti	P	B	S
A709	Bal.	25.09	19.8	1.5	0.9	0.4	0.26	0.15	0.067	<0.01	<0.005	0.0043	<0.001
316	Bal.	10.34	16.05	2.1	1.7	0.38	N.D.	0.06	0.066	N.D.	0.035	N.D.	0.024

N. D. = not determined.

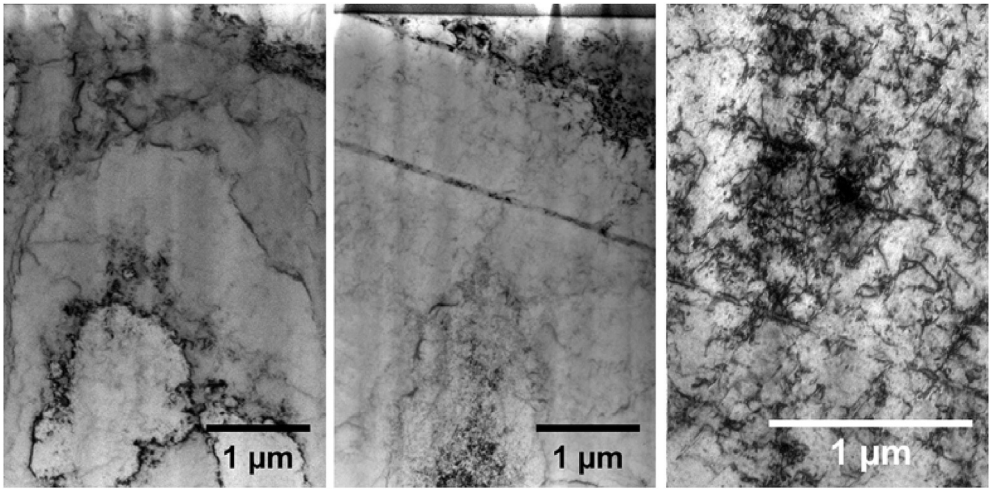

Fig. 1. Twin and dislocation structure of an archive 316 stainless steel hex-block with dislocation densities that are characteristic of light cold-working.

and 400 peak dpa at this temperature, while 316 was irradiated to 100, 200, 300, and 400 peak dpa, also at 575 °C. A peak dose of 400 dpa corresponds to an ion fluence of 3.82×10^{17} ions/cm^2. The maximum injected Fe ion concentration is 10% at the Fe mean projected range.

The microstructure of the irradiated specimens was studied using both bright field transmission electron microscopy (TEM) and scanning transmission electron microscopy (STEM) with a high angle annular dark field (HAADF) detector on a FEI Tecnai F20 ST with an operating voltage of 200 kV. The STEM-HAADF collects scattered electrons from the specimen for imaging at high angles, and therefore voids appear dark in the STEM image. TEM bright field images were mostly used to measure small size voids produced in lower damage level specimens. A previous study showed that void size analyses using TEM bright field and STEM dark field images have good agreement [46].

Microscopy specimens were prepared using a standard focused ion beam (FIB) lift-out technique with the procedure described elsewhere [47]. Thicknesses of the TEM lamellae were measured using a standard electron energy loss spectroscopy (EELS) technique on the FEI Tecnai F20 equipped with a Gatan imaging filter.

2. Results

2.1. Temperature-dependent void swelling

Fig. 2 presents STEM-HAADF micrographs of A709 irradiated to 200 peak dpa at 500, 525, 550, 575 and 600 °C. The void sizes appear to increase monotonically with increasing temperature, while the void densities decrease with increasing temperature, a behavior previously observed in almost all earlier neutron and charged particle studies on austenitic alloys. The solid and dashed curves in Fig. 2e are the calculated normalized dpa profile and the normalized implanted ion profile, respectively, for fully-dense unvoided steel. The damage peaks at ~1000 nm and the Fe ion mean projected range is ~1600 nm. Fig. 2 shows that voids are distributed only within a depth of 800 nm from the surface, a range shallower than the dpa peak depth. Such fore-shortened void distributions are expected and universally observed due to the combined influence of the injected interstitial and defect imbalance effects, as discussed in previous studies [24,27,48]. The implanted Fe ions not only contribute to a local enrichment of the Fe level, but serve as injected extra interstitials, a condition that tends to suppress void nucleation [27,30,31,49].

Fig. 3 shows the average void diameter and void density as a function of irradiation temperature for the 200 peak dpa irradiation, as obtained from STEM characterization. TEM specimens were made from one large grain within the irradiated area to avoid any complexity from grain boundaries. All voids within the whole lamella (~10 μm) are analyzed. Only a limited number of voids were observed for the temperature dependence study due to the relatively low dpa (200) at which this comparison was conducted. On the average, ~23 voids were counted per specimen for the temperature dependence study, thereby contributing to the relatively large error bars. It is clear, however, that the statistics are good enough to clearly show the swelling difference between the two alloys. The error bars are determined by the thickness errors associated with the EELS measurements. The average void diameter and density are averaged over the void-containing range. Void sizes are roughly the same at 500 °C and 525 °C and begin to increase with increasing temperature at T > 525 °C. The void density first increases and then decreases with increasing temperature, with the highest density observed at 525 °C.

Fig. 4a compares depth distributions of void swelling at different temperatures with the normalized fully-dense SRIM-calculated dpa and Fe implant profiles. The maximum void swelling for A709 irradiated to 500, 525, and 550 °C does not exceed 2%, with the swelling peak occurring at a depth between 200 and 400 nm below the surface. At 575 °C, the maximum void swelling reaches ~9% at several depths below 700 nm. The “spike-like” irregularity of the depth profile of swelling is largely an artifact arising from large voids at relatively low void densities, and the fact that the

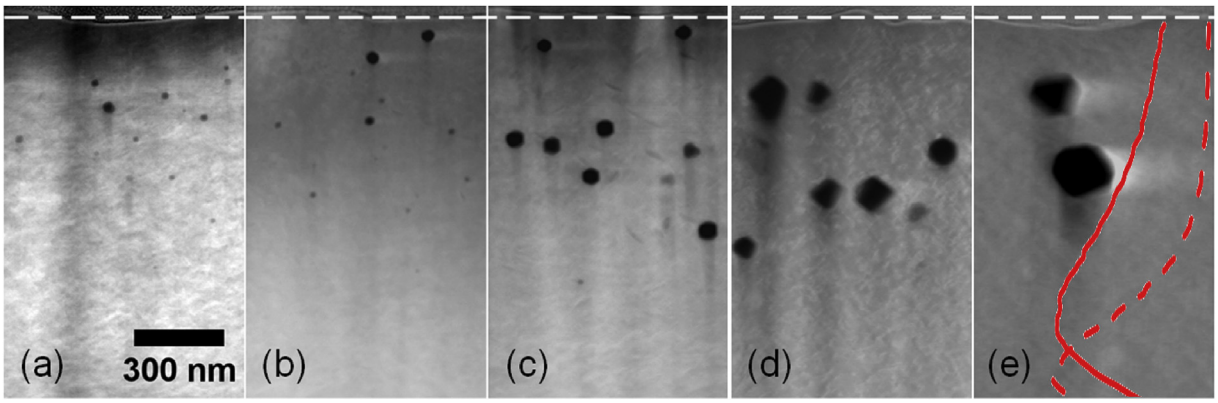

Fig. 2. STEM-HAADF micrographs of A709 irradiated to 200 peak dpa at (a) 500, (b) 525, (c) 550, (d) 575 and (e) 600 °C. The dashed line across the upper part of the figure defines the boundary between the specimen and the platinum coating. The solid and dashed curves in 5e describe the normalized fully-dense unvoided dpa profile and implanted Fe ion profile, respectively.

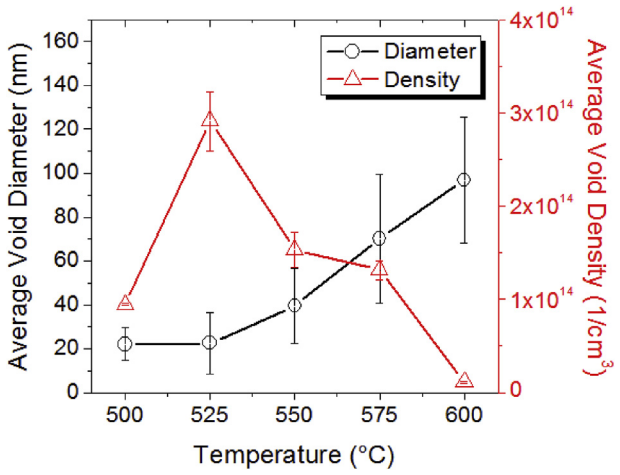

Fig. 3. Average void diameter and density for A709 irradiated to 200 peak dpa at 500, 525, 550, 575, and 600 °C, averaged over the void-containing region.

measuring bin size (100 nm) is comparable to the void size. Most importantly, note that these void distributions inhabit a depth range that is shallow in comparison with the peak of the dpa curve, consistent with previous observations in other alloys [46,47,50].

An increase in the irradiation temperature to 600 °C results in a drop in the maximum swelling to a value of ~4%, with the end of the voided range shifting to a shallower depth of ~400 nm. Fig. 4b compares the swelling (averaged through the void-containing range) as a function of irradiation temperature. 575 °C was determined to be the maximum void swelling temperature (with ~ ±25 °C as the uncertainty range from a Gaussian fitting of Fig. 4b data), reaching ~3.7% of average void swelling, while other temperatures have average swelling less than 1%. Therefore, 575 °C was selected for dose-dependent comparison studies on both A709 and 316. Note that the density and swelling error bars in Fig. 4b were calculated from the sample thickness errors associated with the use of EELS.

2.2. Comparative swelling of A709 and 316 to very high dose

Both A709 and 316 were irradiated to doses as high as 400 peak dpa at 575 °C. Fig. 5a–f shows the STEM micrographs of A709 irradiated to 100, 200, 250, 300, 350, and 400 peak dpa. The solid and dashed curves in each figure represent the normalized fully-dense SRIM-calculated dpa and injected Fe ion profiles, respectively. In general, the void sizes are observed to increase with increasing dose. The void-containing range appears to increase somewhat at higher dose levels. Void denuded zones have formed near the surface and were maintained throughout the irradiation. Due to the irregularity of the surface and the relatively low number of voids in A709, no clear dependence of zone thickness on dose could be established. Note that since the FIB lamellas were lifted out from a single grain, grain-to-grain variations in composition

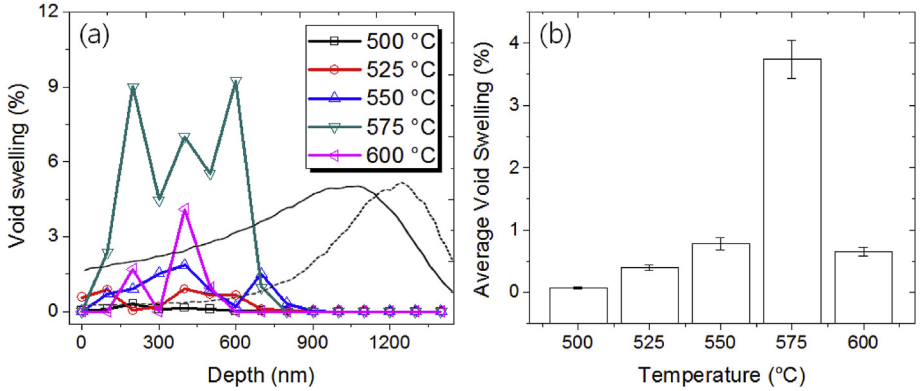

Fig. 4. (a) Depth distribution of void swelling, and (b) depth-averaged void swelling through the void-containing range for A709 irradiated to 200 peak dpa at 500, 525, 550, 575 and 600 °C.

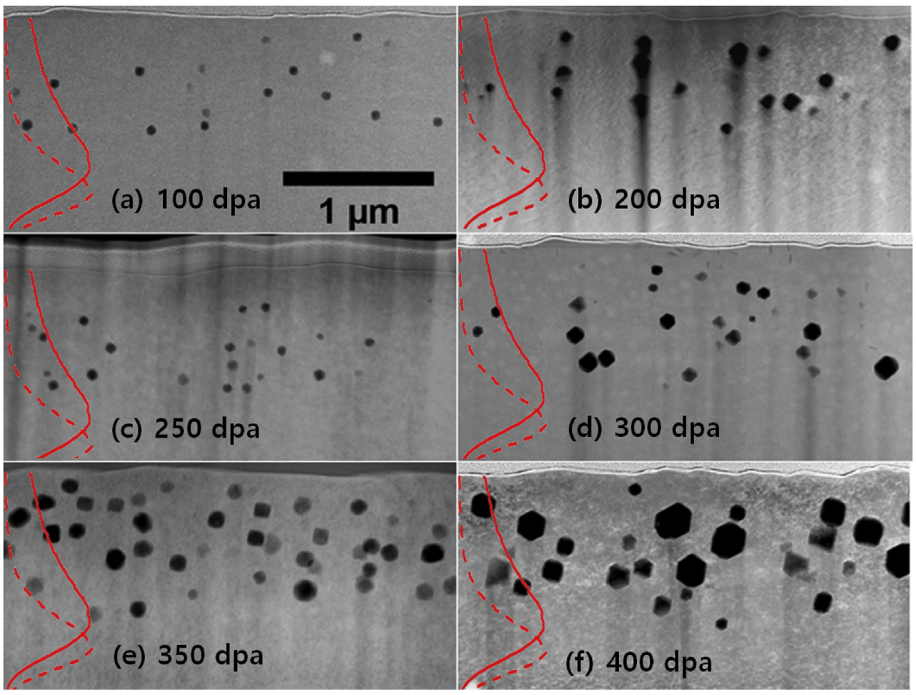

Fig. 5. (a) STEM-HAADF micrographs of A709 irradiated to (a) 100, (b) 200, (c) 250, (d) 300, (e) 350, and (f) 400 peak dpa at 575 °C. Solid and dashed curves superimposed on each image present the normalized fully-dense dpa and injected Fe ion profiles, respectively.

and microstructure may result in fluctuations in void sizes, as seen in Fig. 5b, but the overall void size clearly exhibits a monotonic increase with increasing dpa level.

Fig. 6a–d shows STEM micrographs of 316 irradiated to 100, 200, 300, and 400 peak dpa. The average size of voids increases with increasing dose, similar to the behavior observed in A709. Voids are observed up to 1.35 μm in 400 peak dpa irradiated sample, which is well beyond the SRIM-calculated projected range and to a somewhat lesser extent also beyond the projected range in A709 at 400 dpa. Swelling-induced range extension will be further discussed in the next section. Void denuded zones were also observed near the specimen surface in the 316 specimens, but the zone depth is somewhat variable, perhaps reflecting loss of larger voids though the surface. This observation is similar to behavior seen in high voltage electron irradiations where larger voids near the surface abruptly disappear when they grow into the previously-established denuded zone while smaller voids can nucleate and survive at the same depth [51,52].

Fig. 7a and b compare the average void diameter and density calculated from the 400–700 nm depth region of A709 and 316, respectively, as a function of local dpa (bottom axis) and peak dpa (top axis). On the average 52 and 194 voids were counted per specimen for A709 and 316, respectively, for the dose dependent study. The local dpa values were obtained through averaging the dpa profile over the 400–700 nm region. In Fig. 7a, void sizes in A709 tend to increase with increasing dose after 250 peak dpa (146 local dpa), and the void densities are in a similar range with an exception at 200 peak dpa (116 local dpa) sample. As shown in Fig. 7b, the void sizes of 316 show a consistent rise with increasing dose, while void densities vary with dose and are reduced at >200 dpa. This suggests that voids coalesce at larger void sizes, a frequently observed behavior in many earlier high dose studies

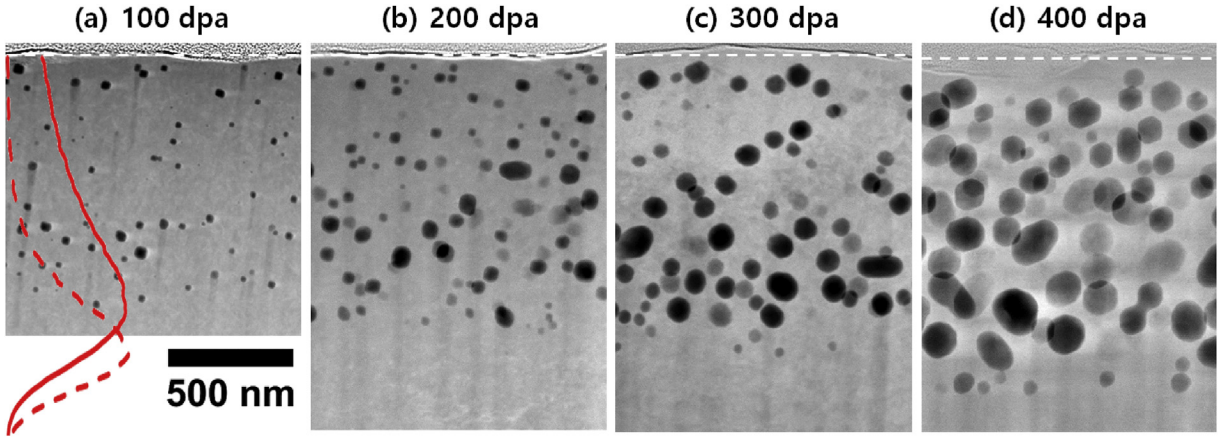

Fig. 6. (a) STEM-HAADF micrographs of 316 irradiated to (a) 100, (b) 200, (c) 300, and (d) 400 peak dpa at 575 °C. The dashed line at the top of the figure defines the boundary between the specimen and the platinum coating. The solid and dashed curves in 5a describe the normalized calculated fully-dense dpa and Fe ion profiles, respectively.

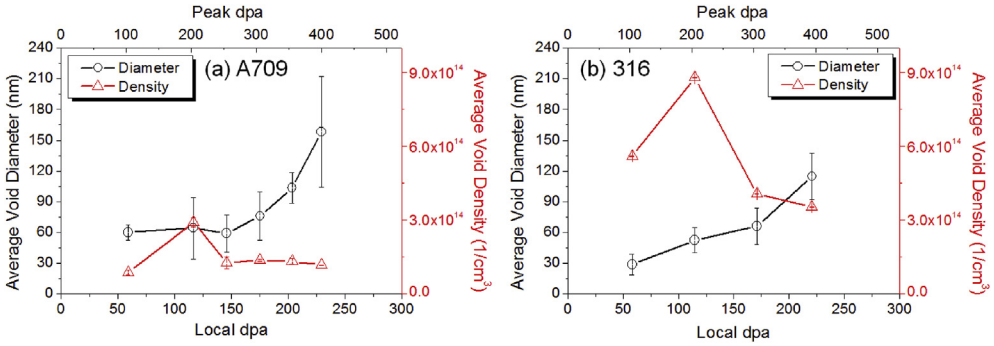

Fig. 7. Depth-averaged void diameters and densities over the 400–700 nm depth region as a function of local dpa (bottom axis) and peak dpa (top axis) of (a) A709, and (b) 316.

using neutrons or charged particles. The void densities of 316 are generally higher than those of A709 at all damage levels, while the void sizes of A709 are generally comparable to those of 316, within the limits of the error bars.

Fig. 8a and b compare void swelling of A709 and 316 at 575 °C, respectively, for various dpa levels as a function of the final actual depth in the specimen. Each STEM micrograph was sectioned into 100 nm bins to extract void swelling data. Fig. 8a shows that the highest swelling level for A709 reaches ~55% at a depth of 550 nm. Despite some variation between various dose levels, the maximum void swelling is located between 400 and 700 nm for A709. In comparison, void swelling at 400 peak dpa for 316 peaks beyond 900 nm, with ~90% swelling in the 750–1000 nm region where injected interstitials normally suppress void nucleation, a finding which cannot be explained by citing only the defect imbalance effect mentioned in previous studies [24,27,48].

Fig. 8 shows that swelling curves extend to deeper depths with increasing dose. The deeper-than-expected void swelling distributions, especially in 316 at 400 dpa, may arise due to density decreases along the ion path, allowing ions to travel further into the material, but depositing less dpa at any given real depth. In effect the local dpa rates are falling with increasing dose. Therefore, a density correction needs to be applied to the fully-dense curves to obtain correct time-averaged local values of dpa.

The necessity of such corrections at higher swelling levels was first discussed by Odette [53] and first experimentally applied by Johnston [54], and later by Mazey [55], but the application of such corrections was found to be rather cumbersome and time-consuming. Getto [56] developed a mass depth correction that was a significant improvement based on the final swelling profiles, but the maximum swelling observed in her paper was only ~16%. A similar mass depth approach was put forward by Wang [28]. However, for our conditions of 55 and 90% swelling for A709 and 316, respectively, a simple mass depth approach is not sufficient, and we need corrections that evolve with time and dose to yield more accurate swelling rates.

2.3. SRIM density correction

The progressive accumulation of swelling requires that the integrated dose at any given real depth be corrected both spatially and temporally. For density correction due to very high void swelling levels, the micrograph of swelling vs. real depth was divided into bins of 100 nm width, and for each layer the local density was revised downward from the fully-dense calculated value using the local void swelling data as shown in Eq. (1),

$$\rho_{corrected} = \left(1 - \frac{\Delta V}{V}\right)\rho_{original} \tag{1}$$

where $\rho_{corrected}$ is a corrected density, $\Delta V/V$ is the void volume fraction, and $\rho_{original}$ is the original density. The original densities used for calculation were 7.99 g/cm^3 for A709 and 7.96 g/cm^3 for 316 obtained from SRIM. Only three major elements, Fe, Cr, and Ni, were included into the SRIM calculation for both alloys to determine the fully-dense dpa curves. Fig. 9 show the differences in SRIM dpa and Fe ion curves at 400 peak dpa before and after density correction. The black solid lines and blue dashed lines refer to the SRIM calculation without using density correction, and the black lines and blue lines, both with squares, refer to the SRIM

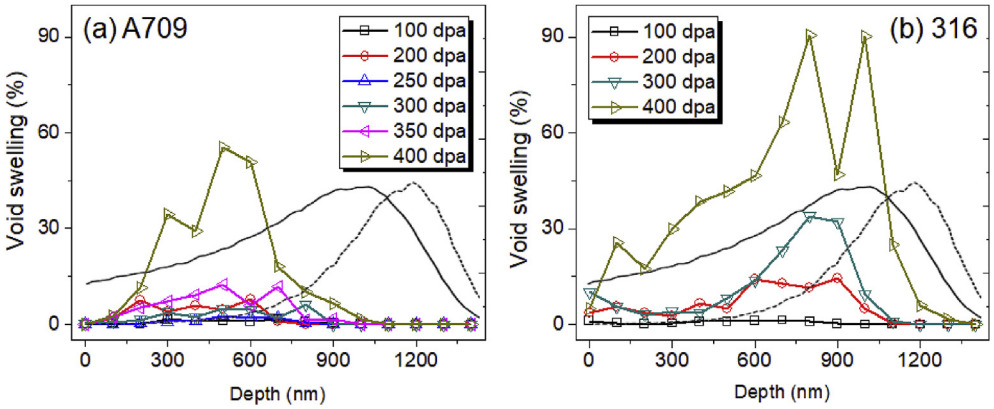

Fig. 8. (a) Depth distribution of void swelling of A709, and (b) 316 irradiated at 575 °C to various damage levels. Normalized fully-dense SRIM-calculated dpa and implanted Fe ion profiles are superimposed with black solid line and dashed line, respectively.

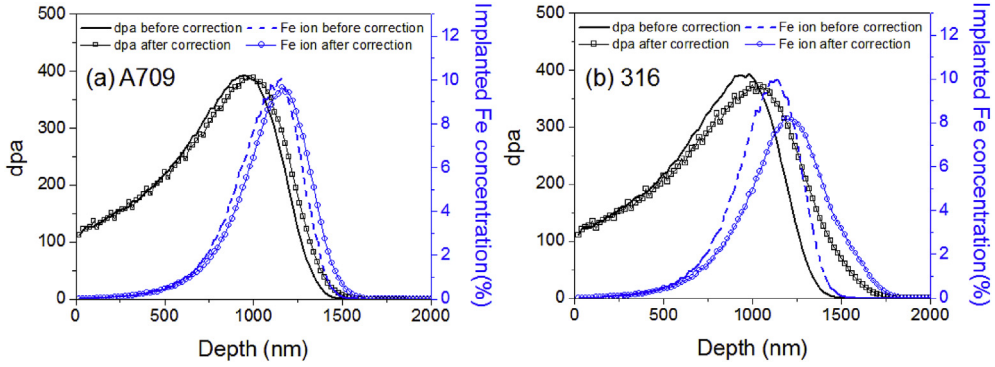

Fig. 9. Dpa and Fe ion profiles of 400 peak dpa before and after density correction for A709 and 316.

calculation after density correction. The difference between before and after correction is more obvious in Fig. 9b, as 316 had much higher void swelling. As shown in Fig. 9b, the dpa and injected Fe ion curves stretch to deeper regions and become broader, explaining why voids were observed in the >1 μm depth region in 316 at 400 original peak dpa.

Fig. 9 shows the maximum profile shift for highest swelling levels at 400 dpa. For interpretation of our very high swelling levels, however, the density correction procedure needs to consider the accumulating impact of swelling during the entire swelling evolution. For this purpose, we divided the total dpa depth range into either 50 dpa or 100 dpa intervals. For each interval, the swelling-induced density change from voids, based on TEM results, was used to obtain corrected dpa profiles for each specific interval. Therefore, the average dpa profile (for different peak damage levels) represents the summed contributions of each dpa interval. Fig. 10a and b shows the corrected dpa profiles for A709 and 316, respectively, with accumulation effects considered. For A709, the dpa peak is shifted from 950 nm for the 100 peak dpa irradiation to 980 nm for 400 peak dpa, as indicated by the vertical lines in Fig. 10a. In the case of 316, the 100 dpa peak is located at 940 nm and the 400 dpa peak depth is at 1040 nm, producing a 100 nm shift in depth as shown in Fig. 10b. In comparison with A709 dpa curves, 316 dpa curves exhibit a deeper penetration depth, involving more shifting in peak location due to its higher swelling.

In the set of curves in Fig. 11, we can see the swelling vs. dose curves for the uncorrected dose levels (top), followed by the same curves using a Getto-Wang single final dose correction (middle set of curves), and finally on the bottom set we can see the fully-corrected swelling vs. dose curves needed for our very high swelling levels. Comparing the top and bottom set of curves one can see that the correction is largest for the 600–900 nm measurement interval. Using the Getto-Wang final dose correction, however, the corrections yield very unphysical results with negative swelling rates, in effect over-correcting for the void-induced decrease in density.

Fig. 11 presents swelling curves obtained from different depth regions, showing that the transient regime (period before onset of steady-state) of swelling increases in duration with depth. This effect is very obvious for A709 (Fig. 11 e), but not as pronounced for 316 (Fig. 11f). This extension of the transient is thought to be due to the combined effects of the increasing proximity of the injected interstitial distribution with increasing depth and especially the well-known effect of increasing dpa rate to increase the transient duration, observed both in neutron and ion studies. Similar effects have been observed in previous studies on different alloys [1,3,26,58–62]. The difference in flux sensitivity cannot be ascribed to any difference in irradiation conditions and therefore must represent an inherent difference in flux sensitivity of the two alloys, with the difference becoming more pronounced with increasing depth and increasing dpa rate. Since the duration of the transient regime in austenitic steels is known to be sensitive to micro-chemical evolution and precipitation, this would suggest that known flux sensitivities of precipitation (e.g. carbides, gamma prime, G-phase) might account for a difference in flux sensitivity of swelling [1,65].

3. Discussion

There is a big difference in void distributions between A709 and

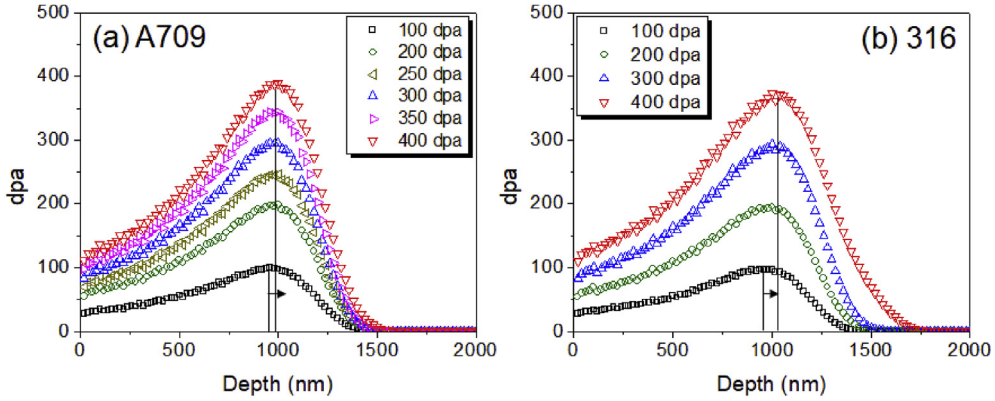

Fig. 10. Density-corrected SRIM dpa curves as a function of depth for A709 and 316. Note the larger shift of the dpa peak depth for higher swelling 316. Vertical lines show the shift of the peak dpa location between 100 and 400 peak dpa.

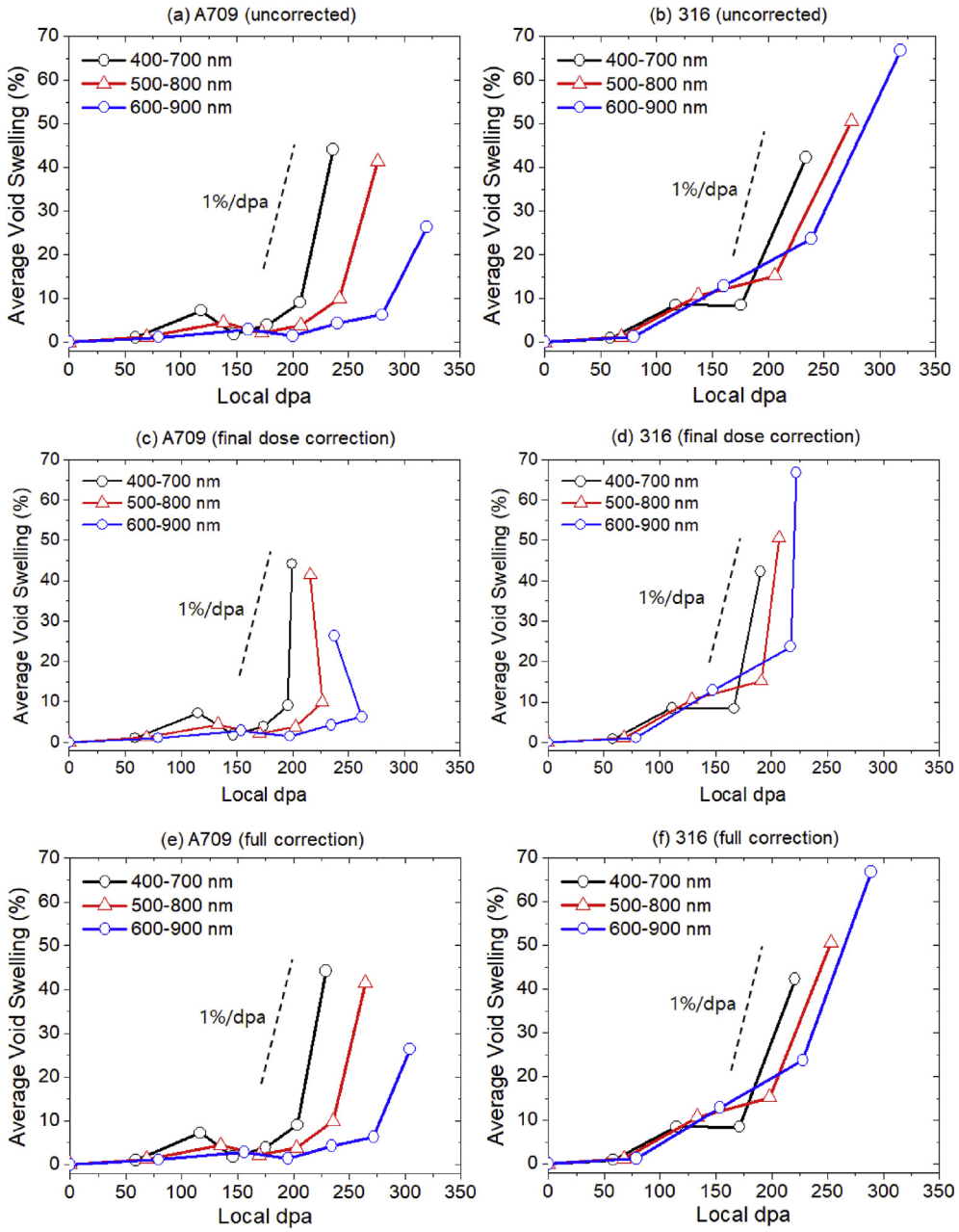

Fig. 11. Three sets of void swelling curves vs. dose of A709 and 316 as a function of local dpa obtained from different depth regions, with no corrections (top), Getto-Wang one step correction (middle) and multiple step corrections (bottom). Swelling data were also collected over different depth regions with correspondingly different average dose rates, since dose rates increase with depth along the ion path. Note that the post-transient swelling rates of both alloys are on the order of ~1%/dpa.

316, especially at the highest dose of 400 peak dpa. As shown in Fig. 8, void swelling in A709 peaks at about 500 nm, which is about half of the projected range. However, void swelling in 316 peaks at much deeper depths, in the depth range of ~750 nm—~1000 nm. Such a difference cannot be explained by swelling-induced density changes. We speculate that the difference primarily arises due to the unique swelling behavior of each alloy.

A recent modeling study by Short et al. has shown a high sensitivity of void nucleation distributions to vacancy migration energy [57]. Under the same irradiation condition in pure Fe, Short showed a small change of vacancy migration energy from 0.83 eV to 0.89 eV causes a dramatic difference in void distribution. At the lower migration energy, the void distribution is similar to the dpa damage curve with a peak close to that of the peak damage. At the higher migration energy, the void distribution peak shifts toward the surface. Short noted that the vacancy migration energy is very sensitive to minor alloying elements such as carbon especially. Whereas Short implicitly assumed that the carbon is in solution, it is important to note that alloys stabilized with carbide formers (Nb, Ti) will have a lower matrix level of carbon. More importantly, while A709 is stabilized with Nb which is absent in 316, but there are significant differences in other minor elements, especially P, S and N that might influence the vacancy migration energy.

We believe there is a correlation between high swelling resistance and shallower void peak location in A709. In the modeling study by Short et al., the surface void removal was not considered, and the model predicts the following trends: the higher the vacancy migration energy, the shallower the void nucleation peak

[57]. Due to the proximity to the surface, a shallower peak also suggests a lower nucleation rate due to surface defect removal effect. Based on these observations, we speculate that A709 may exhibit a higher vacancy migration energy. Although the carbon contents are similar in both alloys, A709 contains 0.26% Nb which effectively reduces the free carbon content. A709 also has a higher Ni content, which may also contribute to this effect, since increased Ni is known to extend the transient regime of swelling, but the differences in Cr and P would tend to partially reverse this effect [63–65]. Given the overall complexity of possible compositional effects it is not possible to conclusively forecast the net effect of the compositional variations.

It is observed that for any data collection interval annealed A709 possesses a longer transient regime than the ~5% cold-worked 316 to enter the high swelling rate regime (the steady state growth stage having a swelling rate of ~1%/dpa). This is significant especially because cold-worked 316 is known to also have a longer transient regime than annealed 316 [1,2], further emphasizing the improved swelling resistance of A709. Once swelling reaches the steady-state growth state, both alloys swell at an ion-induced rate close to 1%/dpa, as expected for face centered cubic (fcc) steels under neutron irradiation [1–3,58,61,63].

4. Conclusion

Alloys A709 and 316 were irradiated with 3.5 MeV self-ion over a range of irradiation temperatures and doses ranging from 100 to 400 dpa, allowing comparative observation of their transient and post-transient swelling behavior. It was demonstrated that A709 has better void swelling resistance than cold-worked 316 during ion irradiation arising from a longer transient regime of swelling, and it is speculated that a similar relationship might occur during neutron irradiation under reactor-relevant conditions. The duration of the transient regime appears also to be flux-sensitive, but different in each alloy, with the difference speculated to arise primarily from the very different compositions producing different rates and kinds of precipitation. Both alloys eventually swelled at an ion-induced rate close to 1%/dpa, as would be expected based on many earlier ion and neutron irradiation studies on austenitic alloys. The proper evaluation of the data generated in this study requires an appreciation of neutron-atypical aspects of ion irradiation. In this study the most important atypical aspects were the injected interstitial suppression of void nucleation and the progressive swelling-induced range extension of the swelling volume, especially at the very large attained swelling levels of 55 and 90% for A709 and 316, respectively. For such large swelling levels, it is important that the swelling-induced decreases in local metal density be introduced taking full account of both the spatial and temporal evolution of the swelling distribution.

Declaration of competing interest

This activity has no conflict of interest with any reviewer or institution.

Acknowledgements

Kim was supported by the US National Science Foundation through grant 1708788. Sham was supported by the U.S. Department of Energy, under Contract No. DE-AC02-06CH11357 with Argonne National Laboratory, managed and operated by UChicago Argonne LLC. The A709 material was procured through the Advanced Reactor Technologies Program of the DOE Office of Nuclear Energy and supplied by the Oak Ridge National Laboratory. The cold-worked 316 material was supplied by D.L. Porter of Idaho National Laboratory.

References

[1] F.A. Garner, Radiation damage in austenitic steels, in: R.J.M. Konings (Ed.), Comprehensive Nucl. Mater, vol. 4, 2012, pp. 33–95.
[2] F.A. Garner, Recent insights on the swelling and creep of irradiated austenitic alloys, J. Nucl. Mater. 122–123 (1984) 459–471.
[3] F.A. Garner, M.B. Toloczko, B.H. Sencer, Comparison of swelling and irradiation creep behavior of fcc-austenitic and bcc-ferritic/martensitic alloys at high neutron exposure, J. Nucl. Mater. 276 (2000) 123–142.
[4] S.J. Zinkle, J.T. Busby, Structural materials for fission & fusion energy, Mater. Today 12 (2009) 12–19.
[5] F.A. Garner, Chapter 10, Void swelling and irradiation creep in light water reactor (LWR) environments, in: P.G. Tipping (Ed.), Understanding and Mitigating Ageing in Nuclear Power Plants, Woodhouse Publishing, 2010, pp. 308–356.
[6] S.J. Zinkle, G.S. Was, Materials challenges in nuclear energy, Acta Mater. 61 (2013) 735–758.
[7] T. Chen, L. Tan, Z. Lu, H. Xu, The effect of grain orientation on nanoindentation behavior of model austenitic alloy Fe-20Cr-25Ni, Acta Mater. 138 (2017) 83–91.
[8] D.S. Smith, N.J. Lybeck, J.K. Wright, R.N. Wright, Thermophysical properties of alloy 709, Nucl. Eng. Des. 322 (2017) 331–335.
[9] B.K. Kim, L. Tan, C. Xu, Y. Yang, X. Zhang, M. Li, Microstructural evolution of NF709 (20Cr-25Ni-1.5MoNbTiN) under neutron irradiation, J. Nucl. Mater. 470 (2016) 229–235.
[10] T. Chen, L. Tan, L. He, B.T. Puschel, K. Sridharan, Microstructural evolution in Fe-20Cr-25Ni austenitic alloys under proton irradiation at 670 °C, Trans. Am. Nucl. Soc. 117 (2017) 581–583.
[11] P.J. Maziasz, B.A. Pint, J.P. Shingledecker, K.L. More, N.D. Evans, E. Lara-Curzio, Austenitic stainless steels and alloys with improved high-temperature performance for advanced microturbine recuperators, in: Proceedings of ASME GT2004-54239 Turbo Expo 2004 Power for Land, Sea, and Air, June 14-17, 2004, pp. 1–13. Vienna, Austria.
[12] H. Naoi, H. Mimura, M. Ohgami, M. Sakakibara, S. Araki, Y. Sogoh, T. Ogawa, H. Sakurai, T. Fujita, Development of tubes and pipes for ultra-supercritical thermal power plant boilers, Nippon Steel Tech. Rep. 57 (1993) 22–27.
[13] C. Xu, W. Chen, Y. Chen, Y. Yang, Microstructural evolution of NF709 austenitic stainless steel under in-situ ion irradiations at room temperature, 300, 400, 500 and 600 °C, J. Nucl. Mater. 509 (2018) 644–653.
[14] J. Stubbins, B. Heuser, P. Hosemann, M. Li, Fundamental studies of irradiation-induced modifications in microstructural evolution and mechanical properties of advanced alloys, Final report for Project No. NEUP 14-6762, April 24 (2018), URL, https://www.osti.gov/biblio/1434640.
[15] H. Mimura, H. Naoi, M. Ohgami, M. Sakakibara, S. Araki, Y. Sogoh, T. Ogawa, H. Sakurai, T. Fujita, Development of tubes and pipes for ultra supercritical thermal power plant boilers, Tech. Rep. 57 (1993) 22–27.
[16] T.-L. Sham, L. Tan, Y. Yamamoto, Development of advanced 9Cr ferritic-martensitic steels and austenitic stainless steels for sodium-cooled fast reactor, in: Proceedings of International Conference on Fast Reactors and Related Fuel Cycles: Safe Technologies & Sustainable Scenarios, Paris, France, March 2013, CN-199-131, International Atomic Energy Agency, Vienna, Austria, 2013.
[17] T.-L. Sham, K. Natesan, Code qualification plan for an advanced austenitic stainless steel, alloy 709, for sodium fast reactor structural applications, in: International Conference on Fast Reactors and Related Fuel Cycles: Next Generation Nuclear for Sustainable Development (FR17), 26-29 June 2017, Yekaterinburg, Russia, IAEA-CN-245-74, 2017.
[18] K. Natesan, X. Zhang, T.-L. Sham, H. Wang, Report on the Completion of the Procurement of the First Heat of Alloy 709, ANL-ART-89, Argonne National Laboratory, Lemont, IL, 2017. June.
[19] X. Liu, J.G. Gigax, Lin Shao, F.A. Garner, J.F. Stubbins, Radiation-induced microstructural evolution and hardening of austenitic alloy 709, Trans. ANS 118 (2018) 1480–1482.
[20] X. Liu, J. G. Gigax, J. D. Poplawsky, W. Guo, H. Kim, L. Shao, F. A. Garner, J. F. Stubbins, Radiation Response of A709 Austenitic Stainless Steel under Fe^{+2} Irradiation at 500 °C, Submitted to Materialia.
[21] G.S. Was, Fundamentals of Radiation Materials Science, Springer, 2007.
[22] G.S. Was, R.S. Averbach, Radiation Damage Using Ion Beams, Comprehensive Nucl. Mater., Elsevier, 2012.
[23] L. Shao, J.G. Gigax, D. Chen, H. Kim, F.A. Garner, J. Wang, M.B. Toloczko, Standardization of accelerator irradiation procedures for simulation of neutron induced damage in reactor structural materials, Nucl. Instrum. Methods Phys. Res. B 409 (2017) 251–254.
[24] L. Shao, C.C. Wei, J. Gigax, A. Aitkaliyeva, D. Chen, B.H. Sencer, F.A. Garner, Effect of defect imbalance on void swelling distributions produced in pure iron irradiated with 3.5 MeV self-ions, J. Nucl. Mater. 453 (2014) 176–181.
[25] F.A. Garner, G.L. Guthrie, The influence of displacement gradients on the interpretation of charged particle simulation experiments, Radiation effects and tritium technology for fusion reactors, CONF-750989 (1976) 491–518.
[26] F.A. Garner, R.W. Powell, D.W. Keefer, et al., Summary report on the alloy development intercorrelation program experiment, in: Proceedings of Workshop on Correlation of Neutron and Charged Particle Damage, Oak

Ridge, TN, 1976, pp. 147–175.
[27] F.A. Garner, Impact of the injected interstitial on the correlation of charged particle and neutron-induced radiation damage, J. Nucl. Mater. 117 (1983) 117–197.
[28] J. Wang, M.B. Toloczko, N. Bailey, F.A. Garner, J. Gigax, L. Shao, Modification of SRIM-calculated dose and injected ion profiles due to sputtering, injected ion buildup and void swelling, Nucl. Instrum. Methods Phys. Res. B 387 (2016) 20–28.
[29] F.A. Garner, G.L. Wire, E.R. Gilbert, Stress effects in ion-bombardment experiments, in: Radiation Effects and Tritium Technology for Fusion Reactors, CONF-750989, 1976 pp. I–474.
[30] A.S. Kumar, F.A. Garner, in: F.A. Garner, J.S. Perrin (Eds.), Dual Ion Irradiation: Impact of the Conflicting Roles of Helium on Void Nucleation, Effects of Radiation on Materials: Twelfth International Symposium, ASTM STP 870, ASTM, Philadelphia, PA, 1985, pp. 493–506.
[31] M.P. Short, D.R. Gaston, M. Jin, L. Shao, F.A. Garner, Modeling injected interstitial effects on void swelling in self-ion experiments, J. Nucl. Mater. 471 (2015) 200–207.
[32] Y. Huang, J.M.K. Wiezorek, F.A. Garner, P.D. Freyer, T. Okita, M. Sagisaka, Y. Isobe, T.R. Allen, Microstructural characterization and density change of 304 stainless steel reflector blocks after long-term irradiation in EBR-II, J. Nucl. Mater. 465 (2015) 516–530.
[33] F.A. Garner, T. Okita, Y. Isobe, J. Etoh, M. Sagisaga, T. Matsunaga, P.D. Freyer, Y. Huang, J.M.K. Wiezorek, D.L. Porter, Measurement of depth-dependent swelling in thick non-uniform irradiated 304 stainless steel blocks using nondestructive ultrasonic techniques, in: Proceedings of Fontevraud 8 - Contributions of Materials Investigations and Operating Experience to LWR's Safety, Performance and Reliability, Avignon, France, 2014.
[34] J.G. Gigax, E. Aydogan, T. Chen, D. Chen, L. Shao, Y. Wu, W.Y. Lo, Y. Yang, F.A. Garner, The influence of ion beam rastering on the swelling of self-ion irradiated pure iron at 450 °C, J. Nucl. Mater. 465 (2015) 343–348.
[35] E. Getto, Z. Jiao, A.M. Monterrosa, K. Sun, G.S. Was, Effect of irradiation mode on the microstructure of self-ion irradiated ferritic-martensitic alloys, J. Nucl. Mater. 465 (2015) 116–126.
[36] R. Stoller, M.B. Toloczko, G.S. Was, A.G. Certain, S. Dwaraknath, F.A. Garner, On the use of SRIM for computing radiation damage exposure, Nucl. Meth. Phys. Res. Sect. B 310 (2013) 75–80.
[37] J.F. Ziegler, M.D. Ziegler, J.P. Biersack, SRIM – the stopping and range of ions in matter (2010), Nucl. Instrum. Methods Phys. Res. B 268 (2010) 1818–1823.
[38] J.G. Gigax, H. Kim, E. Aydogan, F.A. Garner, S. Maloy, L. Shao, Beam-contamination-induced compositional alteration and its neutron-atypical consequences in ion simulation of neutron-induced void swelling, Mater. Res. Lett. 5 (7) (2018) 478–485.
[39] L. Shao, J.G. Gigax, H. Kim, F.A. Garner, J. Wang, M.B. Toloczko, Carbon contamination, its consequences and its mitigation in ion-simulation of neutron-induced swelling of structural metals, in: Proceedings of the 18th International Conference on Environmental Degradation of Materials in Nuclear Power Systems–Water Reactors, The Minerals, Metals & Materials Series, 2017, pp. 681–693.
[40] J.G. Gigax, H. Kim, E. Aydogan, L.M. Price, X. Wang, S.A. Maloy, F.A. Garner, L. Shao, Impact of composition modification induced by ion beam Coulomb-drag effects on the nanoindentation hardness of HT9, Nucl. Instrum. Methods Phys. Res. B 444 (2019) 68–73.
[41] E. Getto, G. Vancoevering, G.S. Was, The co-evolution of microstructure features in self-ion irradiated HT9 at very high damage levels, J. Nucl. Mater. 484 (2017) 193–208.
[42] E. Getto, K. Sun, G.S. Was, Characterization of M_2X formed during 5 MeV Fe^{2+} irradiation, J. Nucl. Mater. 485 (2017) 154–158.
[43] S. Taller, D. Woodley, E. Getto, A.M. Monterrosa, Z. Jiao, O. Toader, F. Naab, T. Kubley, S. Dwaraknath, G.S. Was, Multiple ion beam irradiation for the study of radiation damage in materials, Nucl. Instrum. Methods Phys. Res. B 412 (2017) 1–10.
[44] A.M. Monterrosa, D. Woodley, Z. Jiao, G.S. Was, The influence of carbon on cavity evolution in ion-irradiated ferritic-martensitic steels, J. Nucl. Mater. 509 (2018) 722–735.
[45] J. Wang, M.B. Toloczko, K. Kruska, D.K. Schreiber, D.J. Edwards, Z. Zhu, J. Zhang, Carbon contamination during ion irradiation - accurate detection and characterization of its effect on microstructure of ferritic/martensitic steels, Sci. Rep. 7 (2017) 15813.
[46] C. Zheng, D. Kaoumi, Radiation-induced swelling and radiation-induced segregation & precipitation in dual beam irradiated Ferritic/Martensitic HT9 steel, Mater. Char. 134 (2017) 152–162.
[47] J.G. Gigax, T. Chen, H. Kim, J. Wang, L.M. Price, E. Aydogan, S.A. Maloy, D.K. Schreiber, M.B. Toloczko, F.A. Garner, L. Shao, Radiation response of alloy T91 at damage levels up to 1000 peak dpa, J. Nucl. Mater. 482 (2016) 257–265.
[48] A.D. Brailsford, L.K. Mansur, Effect of self-ion injection in simulation studies of void swelling, J. Nucl. Mater. 71 (1977) 110–116.
[49] D.L. Plumpton, W.G. Wolfer, Suppression of void nucleation by injected interstitials during heavy ion bombardment, J. Nucl. Mater. 120 (1984) 245–253.
[50] J.G. Gigax, H. Kim, T. Chen, F.A. Garner, L. Shao, Radiation instability of equal channel angular extruded T91 at ultra-high damage levels, Acta Mater. 132 (2017) 395–404.
[51] J.J. Laidler, F.A. Garner, L.E. Thomas, Simulation experiments with the high voltage electron microscope, in: Proc. Of ASM Materials Science Seminar, Radiation Damage in Metals, Nov. 9-10, 1975, pp. 194–226. Cincinnati, Ohio.
[52] A. Hishinuma, Y. Katano, K. Shiraishi, Surface effect on void swelling behavior of stainless steel, J. Nucl. Sci. Technol. 14 (1977) 664–672.
[53] G.R. Odette, D.M. Schwartz, A.G. Ardell, Particle range and energy deposition in materials containing voids, Radiat. Eff. 22 (1974) 217–223.
[54] W.G. Johnston, J.H. Rosolowski, A.M. Turkalo, T. Lauritzen, The depth distribution of void swelling produced by 5 MeV Ni ions, J. Nucl. Mater. 62 (1976) 167–180.
[55] D.J. Mazey, J.A. Hudson, S. Nelson, The dose dependence of void swelling in A.I.S.I. 316 stainless steel during 20 MeV C^{++} irradiation at 525 °C, J. Nucl. Mater. 41 (1971) 257–273.
[56] E. Getto, K. Sun, S. Taller, A.M. Monterrosa, Z. Jiao, G.S. Was, Methodology for determining void swelling at very high damage under ion irradiation, J. Nucl. Mater. 477 (2016) 273–279.
[57] M.P. Short, D.R. Gaston, M. Jin, L. Shao, F.A. Garner, Modeling injected interstitial effects on void swelling in self-ion irradiation experiments, J. Nucl. Mater. 471 (2016) 200–207.
[58] T. Okita, N. Sekimura, F.A. Garner, L.R. Greenwood, W.G. Wolfer, Y. Isobe, Neutron-induced microstructural evolution of Fe-15Cr-16Ni alloys at ~ 400°C during neutron irradiation in the FFTF fast reactor, in: 10th International Conference on Environmental Degradation of Materials in Nuclear Power Systems – Water Reactors, 2001 issued on CD format, no page numbers.
[59] T. Okita, N. Sekimura, T. Iwai, F.A. Garner, Investigation of the synergistic influence of irradiation temperature and atomic displacement rate on the microstructural evolution of ion-irradiated model austenitic alloy Fe-15Cr-16Ni, in: 10th International Conference on Environmental Degradation of Materials in Nuclear Power Systems – Water Reactors, 2001 issued on CD format, no page numbers.
[60] T. Okita, N. Sekimura, T. Sato, F.A. Garner, L.R. Greenwood, The primary origin of dose rate effects on microstructural evolution of austenitic alloys during neutron irradiation, J. Nucl. Mater. 307–311 (2002) 322–326.
[61] T. Okita, W.G. Wolfer, T. Sato, N. Sekimura, F.A. Garner, Influence of composition, helium generation rate and dpa rate on neutron-induced swelling of Fe-15Cr-1Ni-0.25Ti alloys, in: FFTF at ~400°C, 11th International Conference on Environmental Degradation of Materials in Nuclear Power Systems – Water Reactors, 2003, pp. 657–663.
[62] T. Okita, T. Sato, N. Sekimura, T. Iwai, F.A. Garner, The synergistic influence of temperature and displacement rate on microstructural evolution of ion-irradiated Fe-15Cr-16Ni model austenitic alloy, J. Nucl. Mater. 367–370 (2007) 930–934.
[63] F.A. Garner, H.R. Brager, in: F.A. Garner, J.S. Perrin (Eds.), Swelling of Austenitic Fe-Cr-Ni Ternary Alloys during Fast Neutron Irradiation, Effects of Radiation on Materials: Twelfth International Symposium, ASTM STP 870, ASTM, Philadelphia, PA, 1985, pp. 187–201.
[64] F.A. Garner, A.S. Kumar, in: F.A. Garner, N.H. Packan, A.S. Kumar (Eds.), The Influence of Both Major and Minor Element Composition on Void Swelling on Simple Austenitic Steels, Effects of Radiation on Materials: Thirteenth International Symposium (Part 1) Radiation-Induced Changes in Microstructure, ASTM STP 955, ASTM, Philadelphia, PA, 1987, pp. 289–314.
[65] F.A. Garner, T. Lauritzen, M.A. Mitchell, The complex action of major solutes on radiation induced swelling of Fe-Cr-Ni austenitic alloys, in: Proceedings of 16th ASTM International Symposium on Effects of Radiation on Materials, ASTM STP 1175, Denver, CO, June 22-24, 1992, pp. 803–815.